Parameter Identification and Evaluation of a Proportional Directional Flow Control Valve Model

J van der Merwe, JH Muller and C Scheffer

Received 13 February 2013, received in revised form 10 June 2013 and accepted 13 September 2013

Servo-pneumatic command device selection and control may be greatly aided by adequate mathematical models and identification procedures. This paper reports on theory and experimental procedures applicable to the characterisation of pneumatic proportional directional flow control valves. The model implemented is shown to be well suited to predicting the effects that sharp-edged, concatenated orifices and small openings have on mass flow. An experimental setup and test protocol is presented that is less wasteful in terms of energy and effort than that of the ISO 6358:1989(E) standard. Unknown model parameters are optimised during the identification procedure, characterising the behaviour of the valve for the entire range of control signal inputs. The identified model yields adequate results, with mean absolute error (MAE) values of less than 10 kPa in the presence of 700 kPa supply pressure for quasi-static control signal inputs. Acceptable prediction is also achieved for the transient control input case investigated. The work presented here then not only serves as a thorough introduction to proportional servo valve modelling theory and identification but may also prove suitable for use in a multitude of practical applications.

Additional keywords: Modelling, pneumatic systems, proportional valves

Nomenclature

Roman

A	Effective orifice area [m^2]
a	Cracking pressure ratio
b	Critical pressure ratio
C	Sonic conductance [$m^3.Pa^{-1}.s^{-1}$]
C_d	Discharge coefficient
D_h	Nominal bore diameter [m]
f_i	Predicted model value
MAE	Mean absolute error
$\dot{m}$	Mass flow rate [$kg.s^{-1}$]
n	Number of elements
P_a	Absolute atmospheric pressure [Pa]
P_d	Absolute downstream pressure [Pa]
Pu	Absolute upstream pressure [Pa]
$\dot{P}_v$	Rate of vessel pressure change [$Pa.s^{-1}$]
R	Gas constant [$J.kg^{-1}.K^{-1}$]
T_0	Atmospheric reference temperature [K]
u	Control signal input [V]
V	Volume [m^3]
y_i	Recorded experimental value

Greek

α_i	Heat transfer coefficient
β	Subsonic flow index
γ	Ratio of specific heats
ρ_0	Atmospheric reference density [$kg.m^{-3}$]
ψ	Flow function

All the authors are from the Department of Mechanical and Mechatronic Engineering, Stellenbosch University, Stellenbosch, South Africa. E-mail: cscheffer@sun.ac.za

1. Introduction

Pneumatic circuits consist of an actuator, a command device and connectors. Compressed air is employed as a medium with which to store or transfer energy. In order to improve accuracy and aid system design and controller development, accurate models of the various components that make up such circuits are required. This paper focuses on command devices, in particular proportional directional flow control valves.

St Venant and Wantzel first derived the relation for mass flow through an ideal, well-rounded orifice in 1839[1]. Servo-pneumatic valve modelling has subsequently seen considerable development. A discharge coefficient was included to adapt said equations for flow through thin, sharp-edged orifices[2]. The subsonic portion of the flow function was approximated by a quarter section of an ellipse. This facilitates the modelling of a concatenated series of orifices, considered to be a better approximation of most commercially available valves[2]. Finally, the flow function has then been modified in order to account for a phenomenon such as the cracking pressure ratio[3, 4].

Though derived for constant orifice openings, the mass flow model has been successfully applied to proportional valves[4, 5, 6]. This has mostly, however, formed part of a larger study concerned with the modelling of an entire pneumatic circuit. The literature regarding such valves is therefore scant, and much information that may have proven helpful is lacking.

Presented in this paper therefore is an overview of theory applicable to servo valves. The additions and modifications to the original orifice model are presented and motivated in sequence. Furthermore, an experimental setup derived from the literature[4, 7] is used for data acquisition. Said setup is less wasteful in terms of compressed air and simpler to implement than the method detailed in the ISO 6358:1989 standard[2, 7]. An additional feature of the setup used is that it negates the need for a flow meter. Finally, an identification method is discussed, solving for the unknown model parameters.

This study combines aspects from various works in the literature in a heretofore, to the best of the authors' knowledge, unique manner. The result is intended to provide sufficient information on proportional flow control valve theory, modelling and identification in order to serve as a guide for valve selection, control and implementation.

http://www.saimeche.org.za (open access) © SAIMechE All rights reserved.

2. Valve Operation

Proportional directional flow control valves, illustrated conceptually in Figure 1, are used to control pressures within the chambers of a double-acting actuator. A control signal causes the electronics (not shown) to magnetically actuate a coil. This displaces a spool attached thereto in order to vary the airflow through the orifices of the valve. The valve used in this work receives a variable voltage input ranging between 0 and 10 V, with flow closed off at an input of 5 V. Channel A is connected to the supply pressure when the control signal ranges from 5 to 10 V, while Channel B is open to the atmosphere via the exhaust port. The channels switch roles when the signal ranges from values greater than 0 up to 5 V. Also, control signals closer to the neutral input result in smaller orifice openings, while signals closer to either the 0 or 10 V limit yield larger openings.

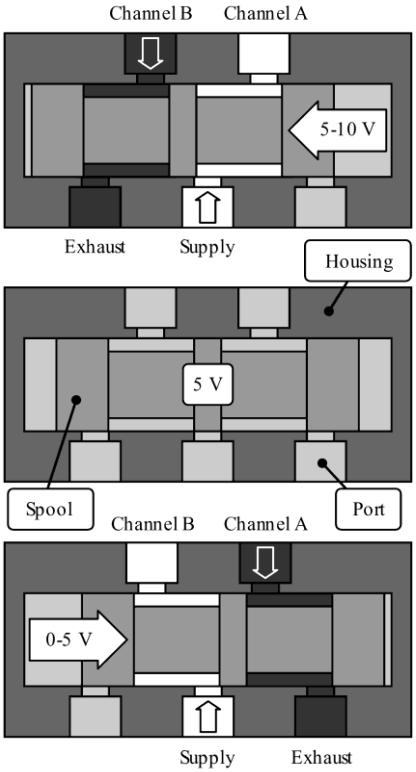

Figure 1: Proportional directional flow control valve function

Note that the dynamics of the spool of the valve is considered negligible due to the large bandwidth of a typical proportional valve, 65 Hz in this case, as compared to the relatively low bandwidth achievable in servo-pneumatic systems, which is not more than 10 Hz[8].

3. Model Theory

For the purposes of this work, it is assumed that all quantities of interest are fully defined throughout the entire air volume and that they vary in a continuous manner between different points in the flow. Atmospheric conditions are taken at the standard technical reference as described by the ISO 6358:1989(E) standard. Furthermore, it is assumed that temperature does not vary from the atmospheric condition during valve operation. While this is not strictly correct, the accuracy of the results obtained validates such a simplified approach.

St Venant and Wantzel first presented the ideal orifice model (1) for free discharge through a well-rounded orifice in 1839[1]. This was derived from first principles under the assumptions that gas behaved ideally, no heat exchange occurred, the upstream pressure and temperature remained constant and the approach velocity was negligible.

$$\dot{m} = A\psi P_u \sqrt{\frac{2}{RT_0}} \tag{1}$$

The subsonic and choked flow regions are modelled collectively by the flow function (3) as a function of the downstream to upstream pressure ratio. Once sonic mass flow velocity is attained, decreasing the values of the pressure ratio below the critical value does not result in an increase of velocity into the supersonic range[2]. Transition between the flow regions is marked by the critical pressure ratio P_{cr} at which the maximum (2) is first reached, as per Figure 2. The values for P_{cr} and ψ_{max} are 0.528 and 0.484, respectively.

$$\psi_{max} = \left(\frac{2}{\gamma+1}\right)^{\frac{1}{\gamma-1}} \sqrt{\frac{\gamma}{\gamma+1}} \tag{2}$$

$$\psi = \begin{cases} \psi_{max} & if \ \frac{P_d}{P_u} \leq P_{cr} \ (choked) \\ \sqrt{\frac{\gamma}{\gamma-1}\left[\left(\frac{P_d}{P_u}\right)^{\frac{2}{\gamma}} - \left(\frac{P_d}{P_u}\right)^{\frac{\gamma+1}{\gamma}}\right]} & if \ \frac{P_d}{P_u} > P_{cr} \ (subsonic) \end{cases} \tag{3}$$

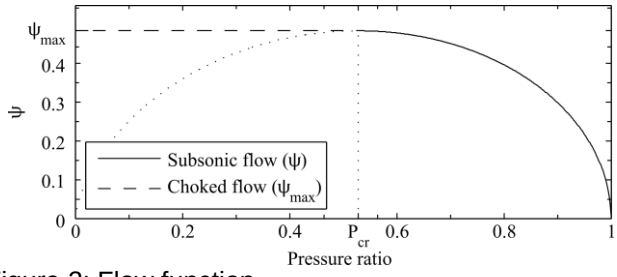

Figure 2: Flow function

Commercial valves, however, do not have ideal orifice geometries, and therefore (1) and (3) must be altered to reflect the effects of such discrepancies. The ideal orifice model (1) is adapted to account for jet contraction, friction, heat losses and other factors that affect a reduction in mass flow rate by introducing a discharge coefficient C_d[2]. This results in the following:

$$\dot{m} = AC_d\psi P_u \sqrt{\frac{2}{RT_0}} \tag{4}$$

Said coefficient is, strictly speaking, a function of the downstream to upstream pressure ratio[2, 9], though a constant has been used with success[5, 10]. Indeed, the ISO 6358:1989(E) standard goes further by lumping C_d together with the area term to obtain the sonic conductance constant (5)[3, 11]. In order to keep the identification procedure simple, C_d will be considered a constant, though kept separate from the area term for the purpose of illustration.

http://www.saimeche.org.za (open access) © SAIMechE All rights reserved.

$$C = \frac{CdA}{\rho_0}\sqrt{\frac{\gamma}{RT_0}\left(\frac{2}{\gamma+1}\right)^{\frac{\gamma+1}{\gamma-1}}} \quad (5)$$

Additional restrictions within the flow path of a valve such as multiple orifices, silencers, connectors and tubing cause the pressure ratio at which sonic velocity is attained to be reduced[2]. To model this effect, the subsonic portion of the flow function (3) is approximated by a quarter section of an ellipse. This allows the introduction of an adjustable critical pressure ratio term b, similar to the model presented in the ISO 6358:1989(E) standard[3, 11].

The flow function is further adapted by introducing the cracking pressure ratio a and subsonic index β parameters[3, 4]. The term 'cracking pressure' stems from the minimum upstream pressure at which a check valve will operate. The inclusion of a accounts for a situation in which flow may cease before the downstream to upstream pressure ratio has reached unity. The subsonic index allows for greater flexibility when modelling a flow path as a concatenated series of orifices as opposed to a single restriction.

The resultant flow function model is given by (6)[3], while the effects of varying the critical and cracking pressure ratios, as well as that of the subsonic index, are illustrated in Figure 3. Along with (4), this then represents the orifice model used henceforth.

$$\psi_e = \begin{cases} \psi_{max} & if \ \frac{P_d}{P_u} \le b \ (choked) \\ \psi_{max}\left[1-\left(\frac{\frac{P_d}{P_u}-b}{a-b}\right)\right]^{\beta} & if \ \frac{P_d}{P_u} > b \ (subsonic) \end{cases} \quad (6)$$

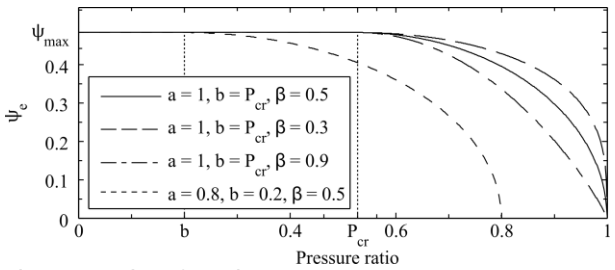

Figure 3: Flow function

4. Experimental Setup

The ISO 6358:1989(E) standard details an experimental setup that may be used to investigate parameters pertaining to mass flow through an orifice. This method requires large amounts of air[2] in addition to a number of experiments to identify parameters for a single orifice opening. The result is a great expense of energy and effort if the flow paths of a proportional valve are to be investigated incrementally across the entire range of the control signal. An alternative setup as shown in Figure 4 is therefore used[4, 7].

The setup consists of a five-port proportional valve (FESTO, MPYE-5-3/8-010-B) connected in series between the supply and a 0.4 L pressure vessel – a single channel is evaluated per test, with the other blocked to negate the effects of leakage. Pressure is measured both within the vessel and at the supply using two transducers (FESTO, SDET-22T-D10-G14-U-M12) with a sensitivity of 9.9 mV.kPa-1 each. The data acquisition unit (National Instruments, cDAQ 9174) employs 16-bit analogue-to-digital (National Instruments, NI 9205) and digital-to-analogue (National Instruments, NI 9264) converters for signal capture and generation purposes. LabView software (National Instruments) running on the desktop computer is used to log incoming data and generate the desired control signal at 1 kHz.

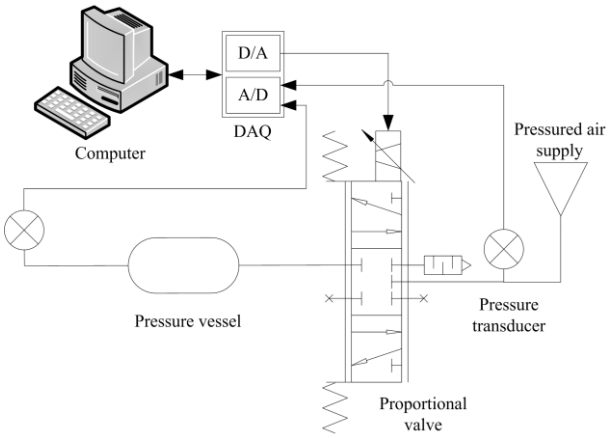

Figure 4: Experimental setup schematic

Note that it may be prudent to perform parameter identification tests on a pneumatic circuit as it would be used in practice instead of attempting to model each component separately. For example, suppose that the valve is employed to control a double-acting cylinder. The channel being investigated could then be connected to one of the chambers of the actuator with the piston rod assembly fixed. This has the advantage of simultaneously modelling all relevant flow restrictions on the path. The result would be a single model detailing the behaviour of the valve, tubing, connectors and other components as a concatenated orifice.

5. Parameter Identification

Parameters that need to be determined are the discharge coefficient C_d, the orifice area A, the critical pressure ratio b, the cracking pressure ratio a and the subsonic index β. The unknown parameters are assumed constant for a particular control signal input. The identification procedure, however, needs to be repeated for each control signal increment across the range for a proportional valve.

Methods have been presented to determine C_d[5, 10], but the manufacturer of the valves (FESTO) has, upon request, supplied a document in which the sonic conductance and critical pressure ratio are listed[12]. These parameters were evaluated in accordance with the ISO 6358:1989(E) standard. It is assumed that these values hold for the maximum geometric orifice area $A_{max} = \pi\frac{1}{4}D_h^2$ and that during testing the inlet and exhaust flow paths were identical. By rewriting (5) the discharge coefficient may then be found.

The critical pressure ratio b will be equal to the corresponding theoretical value of 0.528 for a single, ideal orifice. This is therefore the expected maximum, as any additional restrictions within the flow path will contribute to a reduced b. Should b be negative, choked flow will never occur[4].

The cracking pressure ratio a is considered to be unity for the theoretical and ISO flow function models and

http://www.saimeche.org.za (open access) © SAIMechE All rights reserved.

represents a situation in which the downstream pressure has reached the value of the upstream condition. This will normally be the maximum value, except in certain cases such as when shock waves may develop as a sudden inflow of air reaches an end restriction. The models presented here do not account for this phenomenon. The minimum value of a is calculated by considering atmospheric pressure as downstream with the supply as upstream. Using absolute pressure values, this will never become zero.

Considering the subsonic index β, a value of $\frac{1}{2}$ reproduces the theoretical and ISO flow function models. Otherwise, upper and lower limits of β are difficult to determine as it was introduced purely to increase the flexibility of the extended flow function model[3]. This is opposed to parameters b and a, the addition of which is based on observed phenomena.

In order to determine the unknown parameters, a series of tests using the rig of Figure 4 is performed. Mass flow is not directly measured, negating the need for a flow meter. A model detailing the rate of pressure change within a fixed-volume vessel is instead implemented[5, 6]:

$$\dot{P}_v = \frac{RT_0}{V}\alpha_i \dot{m} \tag{7}$$

For charging, α_i is assumed to have a value close to γ, denoting an adiabatic process, and a value close to one for isothermal behaviour during discharge[5]. Substituting (4) into (7) yields the following:

$$\dot{P}_v = ACd\psi P_u \alpha_i \frac{\sqrt{2RT_0}}{V} \tag{8}$$

Tests were conducted with the supply set at 7 bar absolute pressure. Connecting tubes were kept short in order to support the assumption that flow losses therein were negligible. The control signal is cycled as a square wave in such a manner that the orifice of the relevant channel is opened proportionally either to the supply or to the atmosphere and fully towards the corresponding reverse condition. The particular case depends on whether the inflow or exhaust flow paths are being evaluated.

For Channel A, control signal values of between 5 V and 10 V cause the relevant orifice to open to the supply, while a value of below 5 V connects the pressure vessel to the atmosphere. The square wave is set up with an appropriate bias, amplitude, frequency and duty cycle to ensure that the chamber is fully exhausted before a particular set point is evaluated.

To examine the exhaust flow process, similar tests are conducted. For this case, however, the pressure vessel is considered the source. The vessel is fully charged by an input of 10 V before pressure therein is recorded for control signal values of between 5 V and 0 V as air is exhausted to the atmosphere. Channel B is tested in the same manner, except that the vessel is charged for control signal inputs of between 0 V and 5 V, while discharge occurs for values of between 5 V and 10 V. Figure 5 shows examples of control signals and the recorded vessel pressures for the charge and discharge identification processes of Channel A.

Using the data acquired in this manner, one of Matlab's (MathWorks, Massachusetts, USA) propriety nonlinear least-squares curve-fitting functions, lsqcurvefit, is implemented to simultaneously optimise the parameters discussed. In particular, the function implements a trust region reflective algorithm to fit (8) to a discrete derivative of the vessel pressure curve by minimising the quadratic errors. The termination tolerance is set to 10^{-12}. Unknown parameters are automatically adjusted by the function to achieve a result, with no additional input from the user.

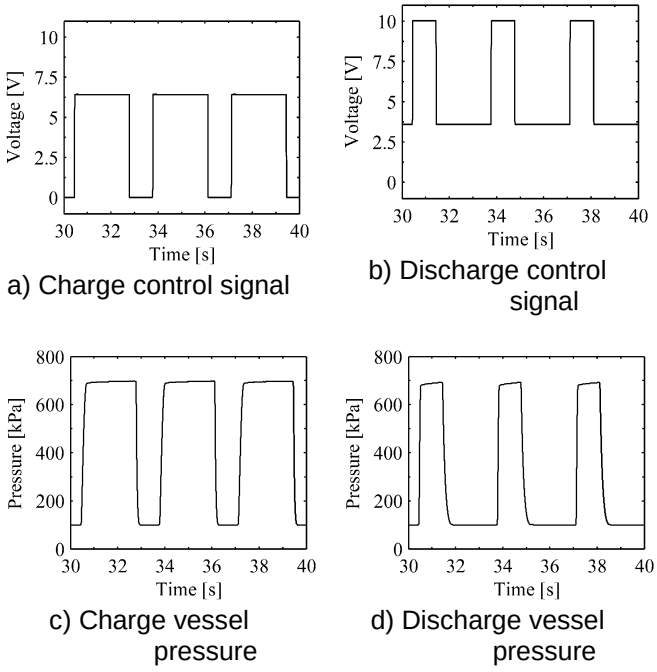

Figure 5: Channel A cyclic test example

Cyclically averaging the data over 10 input signal periods prior to optimisation results in a less noisy signal. Periodic noise is reduced by using a simple moving average filter with a window size of 10 datapoints. Since the region of interest does not include high-frequency components of importance, this allows calculation of the discrete derivative in a manner that does not inhibit the parameter identification procedure.

In order to increase the robustness of the approach, the cracking pressure ratio is predetermined as the maximum recorded value of the downstream to upstream pressure ratio, with an upper limit of unity. Care is taken that the recorded vessel pressure reaches a steady state, which ensures that the cracking pressure limit is indeed reached for small to medium orifice openings. This is accomplished by adjusting the frequency and duty cycle of the control signal accordingly. Furthermore, as C_d is also predefined, the only remaining unknown parameters input to the optimisation algorithm are A, b and β. Their lower limits were all set to zero, with upper limits of 10^{-2}, P_{cr} and 1, respectively.

This process is repeated for each increment of the control signal input across the entire range of the valve for the four cases of charging and discharging of channels A and B.

6. Results

Figure 6 shows the values of the effective orifice area obtained in this manner for both channels. The asymmetric aspect of the curves may be attributed to differing restrictions between the flow paths. Most notably, the exhaust path contains a silencer to reduce noise when the

http://www.saimeche.org.za (open access) © SAIMechE All rights reserved.

system vents to the atmosphere, which the inlet path does not. Note a small offset from the intended neutral position at 5 V, which in reality appears closer to 5.1 V. This may be attributed to manufacturing tolerances within the valve.

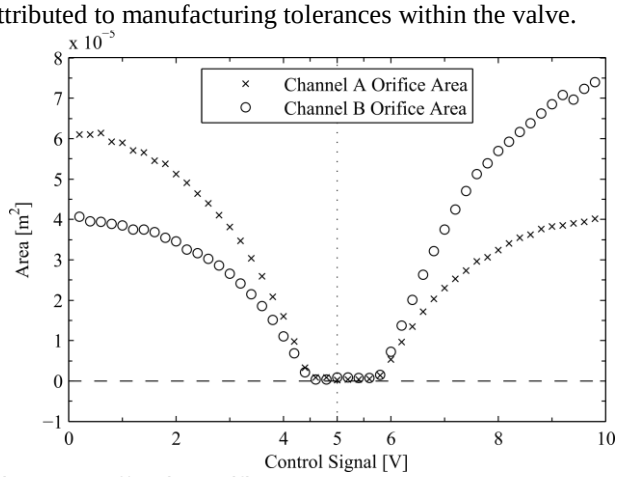

Figure 6: Effective orifice area

The critical and cracking pressure ratios, as well as the subsonic index, remain within the set bounds for optimisation and do not justify plotting versus the control signal. Refer to tables 1 to 5 in the appendix for detailed lists of all identified parameters. Tests beyond the intended charge and discharge control signal ranges for each channel were not conducted. Such tests may serve to quantify the leakage present within the valve.

7. Validation

In order to verify the behaviour of the valve orifice model, the relevant equations and identified parameters for a single channel were implemented in Matlab's Simulink environment. The block diagram is illustrated in Figure 7.

The values of the identified parameters were stored in the lookup tables, with parameter selection occurring via interpolation based on the input signal. Mass flow as per (4) and (6) are modelled in the mflow block, while the rate of pressure change of the fixed volume is calculated within the dtccP block as per (7). Its output is numerically integrated by a fourth order Runge-Kutta formula to obtain the vessel pressure at each successive time step and written to the specified output file. Inputs to the model are the cyclic averages of the control signal and supply pressure from the experimental dataset that is being evaluated.

The performance of the model was evaluated by calculating the mean absolute error (9) for the vessel pressure. A single value was thus obtained, illustrating goodness of fit between the model and each experimental dataset used to identify the unknown parameters.

$$MAE = \frac{1}{n}\sum_{i=0}^{n} |f_i - y_i| \qquad (9)$$

The results are shown in Figure 8. Note that the MAE values are plotted against the relevant control signal amplitude, similar to Figure 6. Also, each plot shows said errors obtained for charging and discharging of the specified channel.

It is apparent that the model presented here performs well for control signals resulting in medium to large orifice openings. In this range the MAE values remain typically well below 5 kPa, which is satisfactory considering that the maximum vessel pressure is equal to that of the supply, namely 700 kPa. For smaller orifice openings, however, the situation deteriorates slightly, with greater errors being present. As previously mentioned, the cracking pressure ratio term is determined by setting a equal to the maximum value of the downstream to upstream pressure ratio obtained from the cyclic average. Premature discharge of the vessel may therefore result in the cracking pressure being set to an erroneous value, as the pressure within the vessel would have continued to rise had it been allowed to. This may be the source of the spikes within the plotted curves of Figure 8.

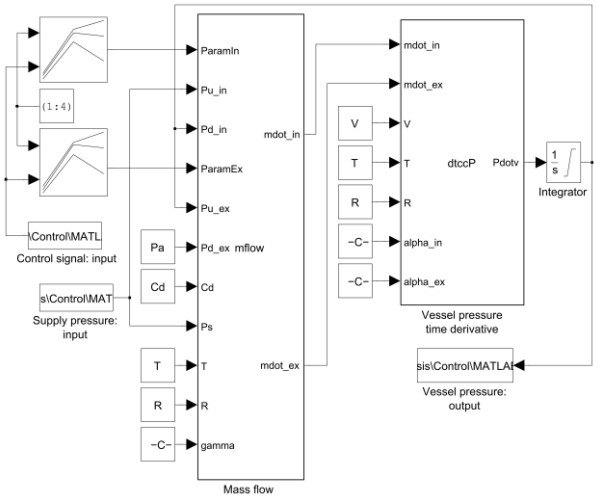

Figure 7: Aeff test setup block diagram

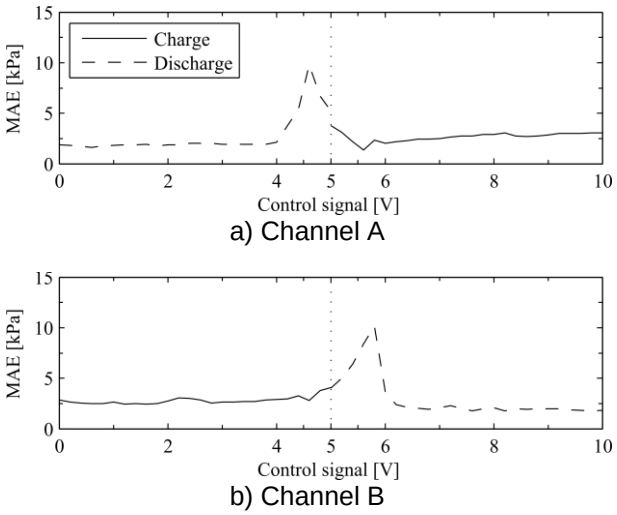

Figure 8: Mean absolute error

Illustrated in Figure 9 are the predicted values of the model superimposed on the test results for small and medium orifice openings, as well as in response to a sinusoidal input. Note that all experimental data were cyclically averaged and smoothed as previously described. From Figure 9(a) one may note the levelling off of the pressure curve at a value less than that of the supply, illustrating the need for the cracking pressure ratio term to accurately model mass flow through small orifice openings. Figure 9(b) also shows adequate model performance for larger orifice openings.

http://www.saimeche.org.za (open access) © SAIMechE All rights reserved.

Figure 9(c) depicts good agreement between the model and experimental data for a control signal set to vary about the 5 V neutral position with an amplitude of 2.5 V and a frequency of 2 Hz. This illustrates to some extent the validity of the model for use in conjunction with transient control signal inputs, even though the identification procedure is based on quasi-static tests.

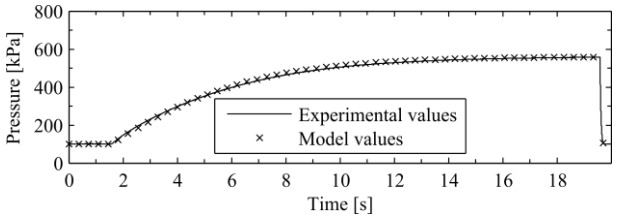

a) Small opening

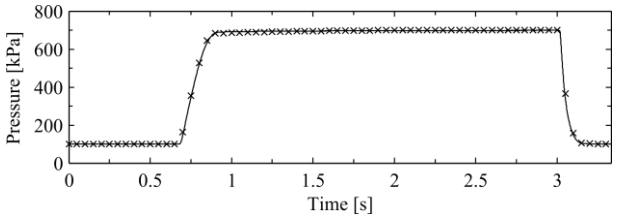

b) Midsize opening

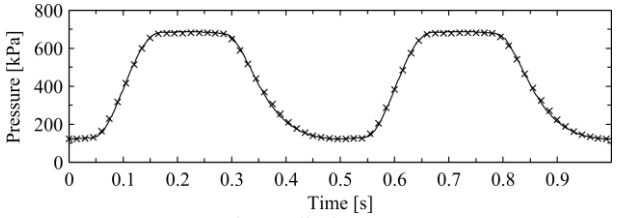

c) Cyclic input

Figure 9: Model verification – Channel A

8. Conclusion

After a summary of relevant model theory, a procedure more suited to identification of the model parameters of a proportional valve than that of the ISO 6358:1989(E) standard is implemented. The effective orifice area, the critical pressure ratio and the subsonic index parameters were optimised simultaneously, with the discharge coefficient and cracking pressure ratio predetermined as discussed to fit vessel pressure data for both inlet and exhaust flow of each channel. Adequate performance is illustrated for quasi-static orifice openings across the entire range of control signals, as well as for a selected transient input.

Acknowledgements

This work was supported by the National Research Foundation of South Africa under Grant SFH2009072300003996.

References

1. *St Venant AJC and Wantzel PL*, Mèmoire et expèriences sur l'ècoulement de l'air, *J. Ecole Polytech*, 1839, 16, 85–122.
2. Beater P, Pneumatic Drives: System Design, Modelling and Control, Springer Verlag, 2007.
3. Harris P, O'Donnel G and Whelan T, Modelling and identification of industrial pneumatic drive system, The International Journal of Advanced Manufacturing Technology, 2012, 58(9-12), 1075–1086.
4. Nouri BMY, Al-Bender F, Swevers J, Vanherek P and Van Brussel H, Modelling a pneumatic servo positioning system with friction, Proceedings of the American Control Conference, 2000, 2, 1067–1071.
5. Richer E and Hurmuzlu Y, A high-performance pneumatic force actuator system: Part I – Nonlinear mathematical model, Journal of Dynamic Systems Measurement and Control, 2000, 122(3), 416–425.
6. Bubert EA, Highly Extensible Skin for a Variable Wing-span Morphing Aircraft Utilizing Pneumatic Artificial Muscle Actuation, MSc thesis, University of Maryland, 2009.
7. Guang-zheng P, Xi-yan, C and Wei F, A new measurement method of the flow-rate characteristics of the regulator, Proceedings of the 6th JFPS International Symposium on Fluid Power, 7-10 November 2005, 766–770.
8. Ning S and Bone GM, Development of a nonlinear dynamic model for a servo pneumatic positioning system, IEEE International Conference on Mechatronics and Automation, 2005, 1, 43–48.
9. Pugi L, Malvezzi M, Allotta B, Banchi L and Presciani P, A parametric library for the simulation of a union internationale des chemins de fer (uic) pneumatic braking system, Proceedings of the Institution of Mechanical Engineers, Part F, Journal of Rail and Rapid Transit, 2004, 218(2), 117–132.
10. Zhu Y, Control of Pneumatic Systems for Free Space and Interaction Tasks with System and Environmental Uncertainties, PhD thesis, Vanderbilt University, 2006.
11. ISO 6358:1989(E), Pneumatic fluid power – Components using compressible fluids – Determination of flow-rate characteristics, ISO, Geneva, Switzerland, 1989.
12. Anon, Proportional-Wegeregelventil MPYE-5-.B, Technical report, Festo, 2006.

Appendix

Table 1: Miscellaneous parameters

Parameter	Value
A_{max}	7.85E-05 m^2
C_d	0.575
D_h	0.01 m
P_a	10^5 Pa
P_{cr}	0.528
T_0	293.15 K
V	0.4 L
α_{in}	1.4
α_{ex}	1
γ	1.4
ρ_0	1.185 $kg.m^{-3}$
ψ_{max}	0.484

http://www.saimeche.org.za (open access) © SAIMechE All rights reserved.

Table 2: Channel A inlet parameters

u	A	b	a	β
0.0	0	5.28E-01	1.000	0.500
0.2	0	5.28E-01	1.000	0.500
0.4	0	5.28E-01	1.000	0.500
0.6	0	5.28E-01	1.000	0.500
0.8	0	5.28E-01	1.000	0.500
1.0	0	5.28E-01	1.000	0.500
1.2	0	5.28E-01	1.000	0.500
1.4	0	5.28E-01	1.000	0.500
1.6	0	5.28E-01	1.000	0.500
1.8	0	5.28E-01	1.000	0.500
2.0	0	5.28E-01	1.000	0.500
2.2	0	5.28E-01	1.000	0.500
2.4	0	5.28E-01	1.000	0.500
2.6	0	5.28E-01	1.000	0.500
2.8	0	5.28E-01	1.000	0.500
3.0	0	5.28E-01	1.000	0.500
3.2	0	5.28E-01	1.000	0.500
3.4	0	5.28E-01	1.000	0.500
3.6	0	5.28E-01	1.000	0.500
3.8	0	5.28E-01	1.000	0.500
4.0	0	5.28E-01	1.000	0.500
4.2	0	5.28E-01	1.000	0.500
4.4	0	5.28E-01	1.000	0.500
4.6	0	5.28E-01	1.000	0.500
4.8	0	5.28E-01	1.000	0.500
5.0	2.93E-07	2.22E-14	0.750	1.000
5.2	3.25E-07	2.22E-14	0.794	1.000
5.4	3.64E-07	2.22E-14	0.835	1.000
5.6	4.35E-07	2.22E-14	0.882	1.000
5.8	1.34E-06	2.34E-14	0.979	0.721
6.0	5.33E-06	3.33E-01	1.000	0.527
6.2	9.61E-06	4.27E-01	1.000	0.490
6.4	1.35E-05	4.21E-01	1.000	0.503
6.6	1.72E-05	4.05E-01	1.000	0.504
6.8	2.03E-05	4.34E-01	1.000	0.510
7.0	2.29E-05	4.77E-01	1.000	0.524
7.2	2.53E-05	5.08E-01	1.000	0.532
7.4	2.74E-05	5.28E-01	1.000	0.533
7.6	2.96E-05	5.28E-01	1.000	0.532
7.8	3.06E-05	5.28E-01	1.000	0.449
8.0	3.25E-05	5.28E-01	1.000	0.448
8.2	3.40E-05	5.28E-01	1.000	0.504
8.4	3.55E-05	5.28E-01	1.000	0.499
8.6	3.63E-05	5.28E-01	1.000	0.476
8.8	3.76E-05	5.28E-01	1.000	0.473
9.0	3.82E-05	5.28E-01	1.000	0.459
9.2	3.85E-05	5.28E-01	1.000	0.439
9.4	3.90E-05	5.28E-01	1.000	0.446
9.6	3.93E-05	5.28E-01	1.000	0.430
9.8	4.02E-05	5.28E-01	1.000	0.449
10.0	3.98E-05	5.28E-01	1.000	0.418

Table 3: Channel A exhaust parameters

u	A	b	a	β
0.0	6.13E-05	3.56E-01	0.988	1.000
0.2	6.10E-05	3.47E-01	0.988	1.000
0.4	6.10E-05	3.38E-01	0.988	1.000
0.6	6.14E-05	3.21E-01	0.988	1.000
0.8	5.92E-05	3.37E-01	0.988	1.000
1.0	5.89E-05	3.25E-01	0.988	1.000
1.2	5.71E-05	3.35E-01	0.988	1.000
1.4	5.65E-05	3.23E-01	0.988	1.000
1.6	5.45E-05	3.26E-01	0.988	1.000
1.8	5.38E-05	3.04E-01	0.988	1.000
2.0	5.12E-05	3.16E-01	0.988	1.000
2.2	4.90E-05	3.08E-01	0.988	1.000
2.4	4.64E-05	3.07E-01	0.988	1.000
2.6	4.40E-05	2.89E-01	0.988	1.000
2.8	4.10E-05	2.77E-01	0.988	1.000
3.0	3.81E-05	2.56E-01	0.988	1.000
3.2	3.47E-05	2.30E-01	0.988	0.992
3.4	3.04E-05	2.10E-01	0.988	0.978
3.6	2.59E-05	1.81E-01	0.988	0.994
3.8	2.08E-05	1.46E-01	0.987	1.000
4.0	1.59E-05	2.22E-14	0.985	1.000
4.2	9.79E-06	2.22E-14	0.963	1.000
4.4	3.33E-06	2.22E-14	0.829	1.000
4.6	8.67E-07	2.22E-14	0.234	1.000
4.8	9.27E-07	2.22E-14	0.200	1.000
5.0	9.96E-07	2.22E-14	0.187	1.000
5.2	0	5.28E-01	1.000	0.500
5.4	0	5.28E-01	1.000	0.500
5.6	0	5.28E-01	1.000	0.500
5.8	0	5.28E-01	1.000	0.500
6.0	0	5.28E-01	1.000	0.500
6.2	0	5.28E-01	1.000	0.500
6.4	0	5.28E-01	1.000	0.500
6.6	0	5.28E-01	1.000	0.500
6.8	0	5.28E-01	1.000	0.500
7.0	0	5.28E-01	1.000	0.500
7.2	0	5.28E-01	1.000	0.500
7.4	0	5.28E-01	1.000	0.500
7.6	0	5.28E-01	1.000	0.500
7.8	0	5.28E-01	1.000	0.500
8.0	0	5.28E-01	1.000	0.500
8.2	0	5.28E-01	1.000	0.500
8.4	0	5.28E-01	1.000	0.500
8.6	0	5.28E-01	1.000	0.500
8.8	0	5.28E-01	1.000	0.500
9.0	0	5.28E-01	1.000	0.500
9.2	0	5.28E-01	1.000	0.500
9.4	0	5.28E-01	1.000	0.500
9.6	0	5.28E-01	1.000	0.500
9.8	0	5.28E-01	1.000	0.500
10.0	0	5.28E-01	1.000	0.500

http://www.saimeche.org.za (open access) © SAIMechE All rights reserved.

Table 4: Channel B inlet parameters

u	A	b	a	β
0.0	4.05E-05	5.28E-01	1.000	0.418
0.2	4.07E-05	5.28E-01	1.000	0.445
0.4	3.95E-05	5.28E-01	1.000	0.425
0.6	3.94E-05	5.28E-01	1.000	0.445
0.8	3.89E-05	5.28E-01	1.000	0.439
1.0	3.85E-05	5.28E-01	1.000	0.458
1.2	3.74E-05	5.28E-01	1.000	0.449
1.4	3.75E-05	5.28E-01	1.000	0.483
1.6	3.68E-05	5.28E-01	1.000	0.503
1.8	3.55E-05	5.28E-01	1.000	0.497
2.0	3.45E-05	5.28E-01	1.000	0.519
2.2	3.25E-05	5.28E-01	1.000	0.454
2.4	3.16E-05	5.28E-01	1.000	0.513
2.6	3.02E-05	5.19E-01	1.000	.546
2.8	2.86E-05	4.81E-01	1.000	0.531
3.0	2.65E-05	4.63E-01	1.000	0.525
3.2	2.41E-05	4.18E-01	1.000	0.507
3.4	2.14E-05	3.74E-01	1.000	0.500
3.6	1.85E-05	3.16E-01	1.000	0.498
3.8	1.51E-05	2.65E-01	1.000	0.479
4.0	1.11E-05	1.96E-01	1.000	0.453
4.2	6.89E-06	2.34E-14	1.000	0.466
4.4	2.13E-06	2.34E-14	0.995	0.733
4.6	4.18E-07	2.22E-14	0.866	1.000
4.8	3.37E-07	2.22E-14	0.805	1.000
5.0	2.96E-07	2.22E-14	0.756	1.000
5.2	0	5.28E-01	1.000	0.500
5.4	0	5.28E-01	1.000	0.500
5.6	0	5.28E-01	1.000	0.500
5.8	0	5.28E-01	1.000	0.500
6.0	0	5.28E-01	1.000	0.500
6.2	0	5.28E-01	1.000	0.500
6.4	0	5.28E-01	1.000	0.500
6.6	0	5.28E-01	1.000	0.500
6.8	0	5.28E-01	1.000	0.500
7.0	0	5.28E-01	1.000	0.500
7.2	0	5.28E-01	1.000	0.500
7.4	0	5.28E-01	1.000	0.500
7.6	0	5.28E-01	1.000	0.500
7.8	0	5.28E-01	1.000	0.500
8.0	0	5.28E-01	1.000	0.500
8.2	0	5.28E-01	1.000	0.500
8.4	0	5.28E-01	1.000	0.500
8.6	0	5.28E-01	1.000	0.500
8.8	0	5.28E-01	1.000	0.500
9.0	0	5.28E-01	1.000	0.500
9.2	0	5.28E-01	1.000	0.500
9.4	0	5.28E-01	1.000	0.500
9.6	0	5.28E-01	1.000	0.500
9.8	0	5.28E-01	1.000	0.500
10.0	0	5.28E-01	1.000	0.500

Table 5: Channel B exhaust parameters

u	A	b	a	β
0.0	0	5.28E-01	1.000	0.500
0.2	0	5.28E-01	1.000	0.500
0.4	0	5.28E-01	1.000	0.500
0.6	0	5.28E-01	1.000	0.500
0.8	0	5.28E-01	1.000	0.500
1.0	0	5.28E-01	1.000	0.500
1.2	0	5.28E-01	1.000	0.500
1.4	0	5.28E-01	1.000	0.500
1.6	0	5.28E-01	1.000	0.500
1.8	0	5.28E-01	1.000	0.500
2.0	0	5.28E-01	1.000	0.500
2.2	0	5.28E-01	1.000	0.500
2.4	0	5.28E-01	1.000	0.500
2.6	0	5.28E-01	1.000	0.500
2.8	0	5.28E-01	1.000	0.500
3.0	0	5.28E-01	1.000	0.500
3.2	0	5.28E-01	1.000	0.500
3.4	0	5.28E-01	1.000	0.500
3.6	0	5.28E-01	1.000	0.500
3.8	0	5.28E-01	1.000	0.500
4.0	0	5.28E-01	1.000	0.500
4.2	0	5.28E-01	1.000	0.500
4.4	0	5.28E-01	1.000	0.500
4.6	0	5.28E-01	1.000	0.500
4.8	0	5.28E-01	1.000	0.500
5.0	8.85E-07	2.22E-14	0.185	1.000
5.2	8.10E-07	2.22E-14	0.195	1.000
5.4	7.50E-07	2.22E-14	0.210	1.000
5.6	7.31E-07	2.22E-14	0.240	1.000
5.8	1.51E-06	2.22E-14	0.639	1.000
6.0	7.23E-06	2.22E-14	0.951	1.000
6.2	1.36E-05	2.22E-14	0.978	1.000
6.4	2.01E-05	2.22E-14	0.984	1.000
6.6	2.63E-05	2.22E-14	0.987	1.000
6.8	3.22E-05	2.22E-14	0.988	1.000
7.0	3.75E-05	2.22E-14	0.988	1.000
7.2	4.24E-05	2.22E-14	0.987	1.000
7.4	4.70E-05	2.22E-14	0.988	1.000
7.6	5.12E-05	2.22E-14	0.988	1.000
7.8	5.38E-05	3.89E-02	0.986	1.000
8.0	5.70E-05	4.80E-02	0.986	1.000
8.2	5.92E-05	7.57E-02	0.987	1.000
8.4	6.16E-05	8.46E-02	0.987	1.000
8.6	6.38E-05	8.43E-02	0.987	1.000
8.8	6.62E-05	7.32E-02	0.987	1.000
9.0	6.85E-05	5.54E-02	0.988	1.000
9.2	7.08E-05	3.54E-02	0.988	1.000
9.4	6.96E-05	1.05E-01	0.988	1.000
9.6	7.24E-05	6.85E-02	0.988	1.000
9.8	7.40E-05	5.90E-02	0.988	1.000
10.0	7.50E-05	5.71E-02	0.988	1.000

http://www.saimeche.org.za (open access) © SAIMechE All rights reserved.